MILLIMETER-WAVES BREAST CANCER IMAGING VIA INVERSE SCATTERING TECHNIQUES

Martina Teresa Bevacqua, Simona Di Meo, Lorenzo Crocco, Tommaso Isernia and Marco Pasian

***Abstract* -** Breast cancer represents one of the main reasons of death among women. As an alternative to the gold standard techniques for breast cancer diagnosis, microwave imaging has been proposed from research community and many microwave systems have been designed mainly to work at low microwave frequencies. Based both on the results of recent dielectric characterization campaigns on human breast *ex-vivo* tissues up to 50 GHz and on the promising feasibility studies of mm-wave imaging systems, in this article, we propose and test inverse scattering techniques as effective tool to process mm-wave data to image breast cancer. Differently from the radar techniques so far adopted in conjunction with mm-wave imaging system, inverse scattering techniques turn out to be more versatile and robust with respect to the reduction of the amount of data and eventually also able to characterize the anomaly in terms of electromagnetic properties. In particular, in the above, two image reconstruction techniques, the Linear Sampling Method and the Born Approximation, are proposed and compared against both simulated and experimental data.

***Keywords* — Born approximation, cancer detection, linear sampling method, inverse scattering problem, microwave imaging, mm-waves breast cancer imaging.**

I. INTRODUCTION[1]

BREAST CANCER is the most common type of cancer among women in the world. It is the fifth most common cause of death from cancer in women and the most frequent cause of death in women in developing countries, as screening programs are almost absent in these areas of the world [1]. The risk of breast cancer doubles every decade until menopause, after which it slowly increases. However, this type of cancer is more common after menopause [1].

Currently, there are some instruments available for the diagnosis and screening of breast cancer. The most common are mammography, ultrasound and breast-magnetic resonance imaging, and, among them, mammography is the gold standard for screening, thanks to its good resolution when dealing with breast with a high fat content (typical of post-menopause [1]-[2]).

However, the research of new technologies for breast imaging is going on, as there are some limitations of the current modalities (for example, the woman exposition to ionizing radiation in mammography, the operator dependence of the ultrasound results and the high costs of breast- magnetic resonance imaging).

Microwave imaging (MWI) is a viable alternative to current imaging modalities, offering a potentially low cost, safe and relatively easy to use systems [3]-[4]. MWI technology is based on the detection of dielectric contrast between healthy and neoplastic tissues [5]-[8]. To this end, microwave systems can be based on the radar and/or tomographic approaches depending on the purpose. The radar approach makes possible to just detect the presence and the relative position of a possible dielectric lesion, while tomography pursues the reconstruction of the dielectric profile of the investigated scenario.

Many prototypes based on both approaches have been proposed over the years [9]-[18] and some have also been tested on patients [9], [14]. However, while these systems demonstrated the working principle for the detection of non-surface targets in ideally all tissue types, they pay the price for the low frequencies involved, with suboptimal resolution especially in breasts with a high fat content, leaving the door open for the possible use of different, higher frequencies [3], [15], [16]. As a matter of fact, the achievable spatial resolution in an MWI system increases when increasing the frequency.

High fat content breasts are typical of post-menopausal women (where the incidence rate of this disease is higher), and this is why they are currently suitable for X-ray imaging. Hence, to overcome the need for women to expose themselves to ionizing radiation and on the basis of the above considerations, as well as considering the good dielectric

This is the post-print version of the following article: M. T. Bevacqua, S. Di Meo, L. Crocco, T. Isernia and M. Pasian, "Millimeter-Waves Breast Cancer Imaging via Inverse Scattering Techniques," in IEEE Journal of Electromagnetics, RF and Microwaves in Medicine and Biology, vol. 5, no. 3, pp. 246-253, Sept. 2021, doi: 10.1109/JERM.2021.3052096. Article has been published in final form at: https://ieeexplore.ieee.org/document/9325514.

contrast between healthy and cancerous tissues even at high frequencies [7]-[8]-[19], the possibility of using frequencies in the millimeter wave regime (20-40 GHz) for the diagnosis of breast cancer in breasts with a high fat content has been proposed, using a radar-based approach [20]-[24]. In particular, in [20], even if the use of higher frequencies poses the problem of strong signal attenuation and worsening of SNR, the authors demonstrated, numerically and with full-wave simulations, the possibility to detect targets with sub-centimetric resolutions up to 4 cm in particularly fat breasts. Moreover, in [23], first experimental images were instead shown. The key point is that using higher frequencies opens the way to the effective diagnosis of early stage (sub-cm) tumors, thus making MWI comparable (and safer) with respect to mammography.

In this respect, the objective of this work is to investigate for the first time the potentialities of tomographic techniques [25] for breast cancer imaging at millimeter-waves frequencies, as well as to emphasize their advantages in term of versatility and robustness with respect to the reduction of the amount of data. Indeed, in the previously adopted radar approaches the achievable resolution is strictly related not only to the central working frequency, but also to the signal bandwidth. Therefore, they require large bandwidths and more amount of data compared to tomographic approaches, in which reasonable resolutions are achieved also with a single frequency or with small signal bandwidths or number of frequencies. This interesting capability of tomographic approaches, together with the one of quantitatively characterizing the tissues, is due to the fact that they rely on a formulation of the imaging task in terms of an inverse scattering problem [25] and take into account the interactions between the electromagnetic signal and the buried objects. This represents a relevant aspect that could imply a less complex and expensive measurement setup as well as a shorter acquisition and processing time.

A preliminary test has been shown in [26], while this paper provides a detailed discussion and a comprehensive collection of simulated and experimental tests, aiming at identifying an anomaly in breast phantom. In particular, the Linear Sampling (LSM) [27] and the Born Approximation (BA) [28] methods are adopted to image targets both in simulations performed with a linear array in air and in fat of 24 antennas in 28 positions (as described below), as well as in experimental tests performed with a linear array involving the same number of antennas in air and in two types of phantom with increasing attenuation values. For both simulations and experimental tests, the results have shown that both methods can allow to correctly identify the target, showing also the superior robustness of the BA in case of lossy and complex scenarios.

The paper is divided as follows. In Section II, after a brief explanation of inverse scattering problem, the Linear Sampling Method and the Born Approximation are described. In Sections III and IV, the results of the simulations and measurements are presented, respectively. Finally, some conclusions are drawn.

II. Methods: Inverse Scattering Techniques for Cancer Detection

With respect to radar ones, the tomographic approaches require an accurate modeling of the scattering phenomena in order to properly take into account the complex interactions between the adopted antennas and the breast, as well as the solution of the underlying inverse scattering problem [25].

The inverse scattering problem aims at retrieving the unknown contrast χ, which encodes both the electromagnetic and geometrical properties of the unknown targets, from the scattered fields measured for a finite number of receiving and transmitting antennas, respectively, N_R and N_T [29]. Such a problem is non-linear and ill-posed. The former circumstance descends from the dependence of the induced contrast sources, or equivalently the total field, on the unknown contrast function χ, while the latter from the compactness of the radiation operator [25],[30].

To overcome such difficulties, several recovery techniques have been introduced in literature. In this paper, breast cancer imaging is performed by means of a 2D inversion procedure by adopting the Linear Sampling [27] and the Born Approximation [28] methods. In particular, LSM and BA are tested for breast cancer detection. Both of them are based on the solution of a linear but ill-posed problem, so that it has to be solved in a regularized sense to avoid instabilities. In order to deal with such issue, in the following, the Tikhonov regularization is considered [30].

More in details, the LSM belongs to the sampling methods, which estimate the target support by sampling the investigation domain in a grid of N points, identified by r. In particular, the discretized version of the LSM linear equation for a fixed frequency and a given point r of the grid which discretizes the investigation domain, reads as [27]:

$$\boldsymbol{K}\boldsymbol{\alpha_t}(\boldsymbol{r}) = \boldsymbol{g_r}(\boldsymbol{r}) \tag{1}$$

wherein $\boldsymbol{\alpha_t}$ represents the $N_T \times 1$ unknown vector, $\boldsymbol{g_r}$ is the $N_R \times 1$ vector containing the values measured at the receiver positions of the field measured when an elementary current is located in the considered point $\boldsymbol{r}$ of the scenario (that is the Green's function). Finally, $\boldsymbol{K}$ is a $N_R \times N_T$ matrix whose generic element is the scattered field at the given frequency. By solving the equation (1) for each point r, we finally obtain a matrix $N_T \times N$ which contains the values of $\boldsymbol{\alpha_t}$. Note that, even if LSM was introduced at the beginning in case of far field data [27], a simple and original physical interpretation has been then proposed in [31], which shows its relationship with electromagnetic focusing problems and allows to extend the method to the case of near field data.

BA faces the inverse scattering problem by solving a convenient linearization of the equation which relates the data and the unknown contrast function χ, that is [28]:

$$\boldsymbol{e_s} = \boldsymbol{L}[\boldsymbol{\chi}(\boldsymbol{r})] \tag{2}$$

wherein $\boldsymbol{L}[\cdot]$ is the discretized version of the Born linear

operator, while $\boldsymbol{\chi}$ is a vector which samples the value of χ over the grid of point discretizing the investigation domain. Finally, $\boldsymbol{e_s}$ is the $(N_R \times N_T) \times 1$ vector which samples the scattered electric field. Note that the linear approximation underlying BA holds true only in case of weak scatterers and/or for objects whose dimension is very small in terms of the wavelength. However, this does not represent a problem as in the following BA is adopted for target identification.

Once the LSM and BA solutions are obtained, the target can be detected by plotting a spatial indicator. In case of LSM, the spatial indicator $\Im_{LSM}(\boldsymbol{r})$ is computed by sampling the investigation domain Ω in different points and evaluating for each point the normalized energy of $\boldsymbol{\alpha_t}$, that is:

$$\Im_{LSM}(\boldsymbol{r}) = \frac{\sum_{t=1}^{N_T} |\boldsymbol{\alpha_t}(\boldsymbol{r})|^2}{\sum_{r=1}^{N_R} |\boldsymbol{g_r}(\boldsymbol{r})|^2} \tag{3}$$

In case of BA, the spatial indicator $\Im_{BA}(\boldsymbol{r})$ is defined as:

$$\Im_{BA}(\boldsymbol{r}) = \frac{|\boldsymbol{\chi}_{BA}(\boldsymbol{r})|}{\sum_{t=1}^{N_T} |\boldsymbol{g_t}(\boldsymbol{r})|^2} \tag{4}$$

wherein $\boldsymbol{\chi}_{BA}$ is the contrast function retrieved by solving equation (2) and $\boldsymbol{g_t}$ is the field radiated in $\boldsymbol{r}$ by a line current at the transmitting antenna position.[2]

Note that, both LSM and BA indicators are normalized with respect to the energy of $\boldsymbol{g_r}$ and $\boldsymbol{g_t}$, respectively, in order to take into account the fact that data are collected only in aspect limited configuration and the medium can be lossy. Indeed, in LSM the field to be matched at the right-hand side of equation (1) becomes progressively less intense when the distance between the sampling point r and the measurement domain grows. In the same line of reasoning, in BA method the incident field becomes less intense when the distance between the observation point r in Ω and the transmitting antenna grows.

In order to improve the quality of the achieved images, both methods take advantages from processing multi-frequency data. Accordingly, multi-frequency indicators can be defined [32],[33]. While LSM requires *a posteriori* combination of the single indicators (3) arising at each frequency, BA can offer the advantage of simultaneously processing the multifrequency data, by defining a multifrequency Born operator. In particular, in the following, even if dielectric properties of tissues depend on frequency, multifrequency BA method is used without adopting a dispersion law, as just target identification is of interest. For more details about multifrequency LSM and BA indicators, the interesting readers are referred to [32]-[33].

[2] For a practical implementation of the methods, in case of antennas acting as transmitters and receivers, for reciprocity $\boldsymbol{g_t} = \boldsymbol{g_r}$.

III. Assessment against Simulated Data

A. Description of simulated scenario

To validate the performance achievable with LSM and BA reconstructions, two linear array scenarios in air and fat were first simulated by using the Ansys Electronics Desktop software. In particular, WR28 antennas were used in both models as radiating elements, with single-mode cut-off frequency of 21.07 GHz and [26.5-40] GHz band. In simulations, the arrays were formed by 28 radiators, spaced half wavelength in the considered medium at 30 GHz (A_{dist}). In the first model (*Simulation1*), the antennas were in air and the target was a metal sphere with a diameter of 2 mm (T_{diam}) at 4 cm from the center of the array (T_{dist}). In the second model (*Simulation2*), the antennas were immersed in a tissue with dielectric properties derived from low-density *ex-vivo* breast tissues (ε'=3 and ε''=0.3 @ 30 GHz, [8]), and the target was a sphere with neoplastic dielectric properties (ε'=19 and ε''=20 @ 30 GHz, [8]) with a diameter of 2 mm at 4 cm from the center of the array. A sketch of the simulated scenario is shown in Figure 1(a).

B. Results

Even if the data have been simulated in a 3D geometry, they have been processed by adopting a 2D scalar inversion procedure, being the aim of this preliminary analysis to demonstrate the possibility of using tomographic approaches for breast cancer detection at mm-waves. In particular, the scattered data has been related to the S-parameters by assuming that each receiving antenna converts the field distribution in its vicinity into a voltage signal whose complex amplitude exactly corresponds to the one of the scattered field. In other words, we are assuming an isotropic receiving antenna having unitary effective length.

Finally, in order to perform a fair comparison, both the LSM and BA indicators have been normalized and plotted over a grid of 40x40 points. In particular, the BA indicator has been normalized to its maximum value, while the LSM indicator has been rescaled as described in [34].

Note that the processing of the dataset of *Simulation1* and *Simulation2*, as well as the one of *Measure 1* described in the Section IV, are relevant in order to understand both the role of losses and the number of processed frequencies, as well as the different performance obtained by LSM and BA.

The results of the assessment with simulated data, that are *Simulation1* and *Simulation2* are shown in Figures 1 and 2, for the first and second model, respectively. As can be seen, in case of air as background medium, both LSM and BA methods can detect the target by processing just a single frequency data; in particular, the maps at 26.5 GHz are shown. In case of antennas and target embedded in a medium with dielectric properties as low-density *ex-vivo* breast tissues, single-frequency data processing is not sufficient to retrieve the target, due to the presence of losses. To overcome such difficulty and also improve the estimation of the target size, a multifrequency inversion procedure is

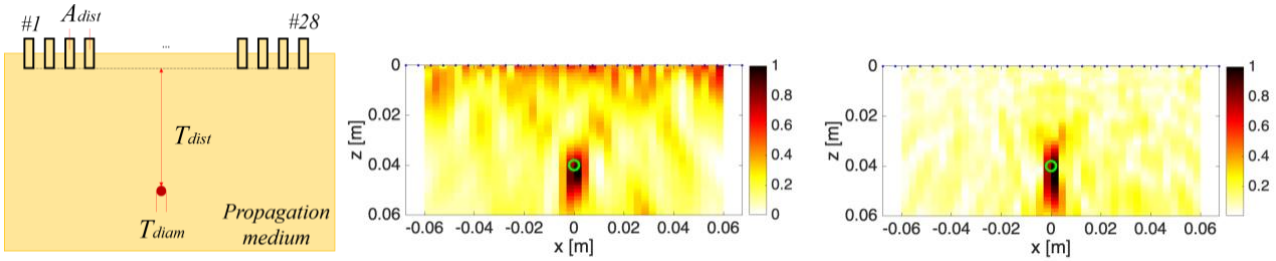

(a) (b) (c)

Figure 1. *Simulation1*. Sketch of the measurement scenario (a). Single-frequency reconstructions at 26.5 GHz. (b) Normalized LSM and (c) BA indicators. The target is superimposed as a green circle, while the antenna positions are depicted as blue points.

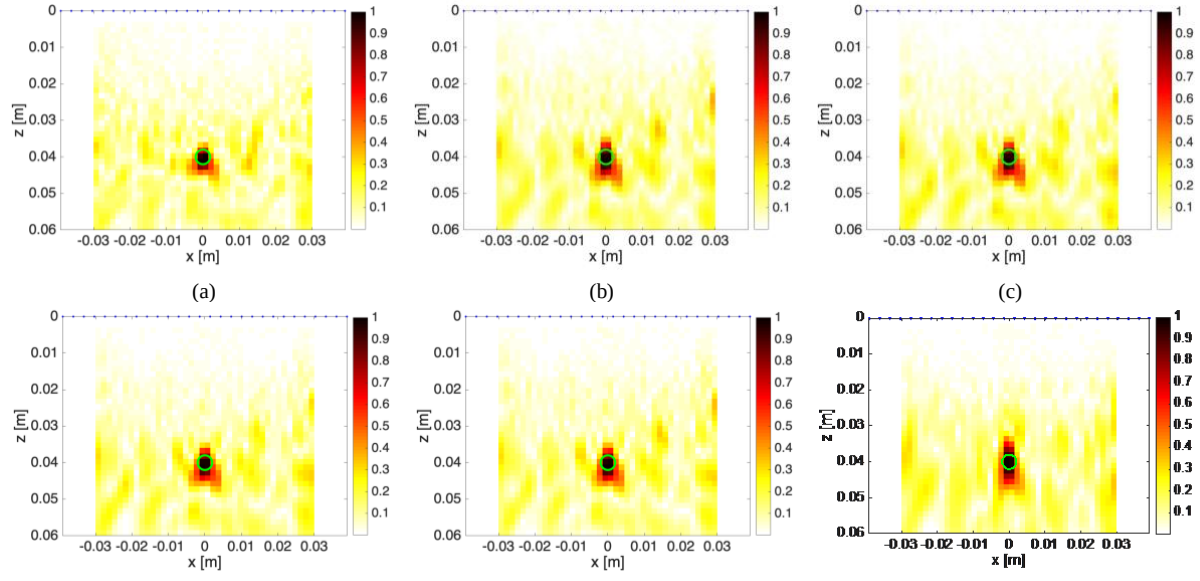

(a) (b) (c)

(d) (e) (f)

Figure 2. *Simulation2*. Normalized multi-frequency BA indicators. (a) [26.5-40] GHz and N_F=271; (b) [26.5-35] GHz and N_F=171; (c) [26.5-35] GHz and N_F=86; (d) [26.5-35] GHz and N_F=30; (e) [26.5-35] GHz and N_F=18; (f) [26.5-32] GHz and N_F=23. The target is superimposed as a green circle, while the antenna positions are depicted as blue points.

adopted. Unlike LSM, due to its capability to simultaneously processing the data, BA indicator is able to make best use of multi-frequency data information, and, hence, detect the target and correctly estimate the target support. This circumstance holds true also in case of reduced number of data (N_F is the number of processed frequencies) and bandwidth, as shown in Figs. 2 (c)-(e). Note that, in Fig. 2, the LSM indicators are not shown as the method is not able to image the target as it does not simultaneously process the data.

IV. Assessment against Experimental Data

A. Description of the experimental setup

After the validation of the LSM and BA performances for the dielectric profile reconstruction of the simulated air and fat scenarios, the two techniques were tested on experimental data. In particular, measurements were first made in air, then with phantom mimicking the dielectric properties of low-density breast tissue with increasing dielectric loss values (e.g., signal attenuations from 0 dB/cm to 1.85 dB/cm).

The experimental setup used for the acquisitions is described in [23] and is summarized here. Two double-ridge antennas (PNR180) with single-mode cut-off frequency of 15.12 GHz and [18-40] GHz band were used to create a synthetic linear array of 24 antennas in 28 positions.

In the experimental tests, the synthetic array was achieved by linearly shifting the two antennas along a predetermined line, with a phase center shift between adjacent radiators equal to half wavelength in air at 30 GHz, 5 mm. Due to the physical dimension of the flange, the spacing between adjacent radiators was limited to 25 mm, justifying the difference between the number of positions and the number of radiators.

The antennas used for experimental tests are a bit different from those used for simulations. In particular, while the highest frequency is 40 GHz in both cases, the lowest working frequency is 26.5 GHz in simulations and 18 GHz in measurements. However, this difference (necessary in simulations to keep the computational effort within the limits of the available workstations) has not any impact on the main purpose of this paper.

The antennas were mounted on four linear translators, allowing them to be positioned in the desired positions, and connected to a two-port PNA Network Analyzer (Keysight

E8361C) via two high-precision coaxial cables. Of the four translators, in the experimental measurements presented in this paper, only two were used to create a linear array and both the positioning of the antennas and the acquisition of signals were controlled by an appropriate MATLAB (The MathWorks, Natick, MA) routine on the PC connected to both the VNA and the four translators. The experimental setup is shown in Figure 3.

Before using the measured radar signals as input for the LSM and BA algorithms, the data were calibrated following the procedure described in [23]. In particular, the crosstalk was eliminated simply by subtracting from the signals measured with the target those measured in air (anechoic panels in front of the antennas), while phase errors were corrected by measuring a reference standard, a metal plate, in the far field region of the antennas.

For measurements in air (*Measure1*), a cylinder with a diameter of 8 mm placed 7 cm from the line of the radiators formed by water and gelatin was used as a target. For measurements with phantoms (*Measure2* and *Measure3*), two types of mixtures based on readily available, low cost and easy-to-handle materials (oil or Polysorbate 80 and waste-oil hardener) with increasing dielectric properties were produced in accordance with [21]-[22] and two standard molds were used for phantoms solidification. In both cases, the targets were water and gelatin cylinders with a diameter of 8 mm placed up to 1.5 cm (d_{target}) deep in the phantoms. The values of the dielectric properties at 30 GHz of both phantoms and the cylindrical inclusion are summarized in Table I. The permittivity of the target used to mimic the dielectric properties of neoplastic tissues is somewhat higher than that of *ex-vivo* malignant tissues. However, the significant dielectric contrast between the target and the background is preserved (e.g., the ratio for ε' is approx. 6.3 for both *ex-vivo* tissues and the case of *Phantom2*). The measurements were made in air, i.e. without coupling medium, with the phantoms placed at about 3.2 cm (*Measure2*) and 5 cm (*Measure3*) from the radiator line ($d_{interface}$). A scheme of the experimental setup is shown in Figure 4.

B. Results

Figures 5-7 show the indicators obtained by processing the experimental data *Measure 1*, *Measure 2*, *Measure 3*. A 2D scalar inversion procedure and a 40x40 grid of points have been considered.

The indicators corresponding to *Measure1* are depicted in Figure 5. In particular, in this figure, image reconstruction at 18 GHz is shown; this frequency even if it is not strictly in the mm-wave regime, it is in the bandwidth of the measured signals. As can be seen, the LSM can detect the target, while its shape and size are not accurately estimated. On the other hand, when BA is adopted, target shape and positions are accurately retrieved, also in case of a reduced number N_F of frequencies (see Figs. 5(e)-(f)). However, if a sufficient number N_F of frequencies is not considered, some artifacts can arise in the indicator map (see the case of N_F=6).

When the second and third scenarios are considered, that are *Measure2* and *Measure3*, both the air-phantom interface[3] and the target are retrieved by means of multifrequency BA processing, as shown in Figures 6 and 7. The LSM indicators are not shown as the method is not able to provide reliable target imaging. As far as the last scenario, it is more cumbersome as $d_{interface}$ is larger and losses are present in the phantom. As a consequence, being weak the signal due to the target, in order to reveal its presence, in Figure 7, we have cut part of the investigation domain above the interface and focused on the bottom part of the picture. As far as the comparison with the radar techniques, the readers are referred to [23].

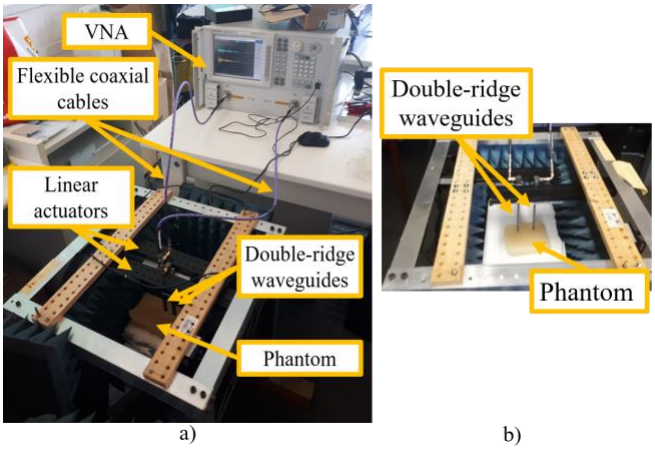

Figure 3. a) Complete experimental setup and b) zoom on antennas and phantoms.

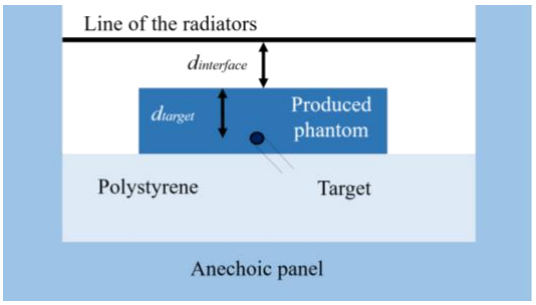

Figure 4. Sketch of the measurement scenario in presence of phantoms.

TABLE I
DIELECTRIC PROPERTIES OF THE PRODUCED PHANTOMS FOR THE TWO MEASUREMENTS AT 30 GHZ [22]-[23]

	ε' [a]	ε'' [a]
Phantom1	2.53 ± 0.11	0 ± 0.14[b]
Phantom2	3.67 ± 0.18	0.13 ± 0.19[b]
Target	23 ± 0.55	24.6 ± 0.28

[a]Mean ± Standard deviation
[b]Only positive values can be considered

[3] This circumstance does not represent a problem, as the contribution of the interface can be avoided by conveniently pre-processing the data.

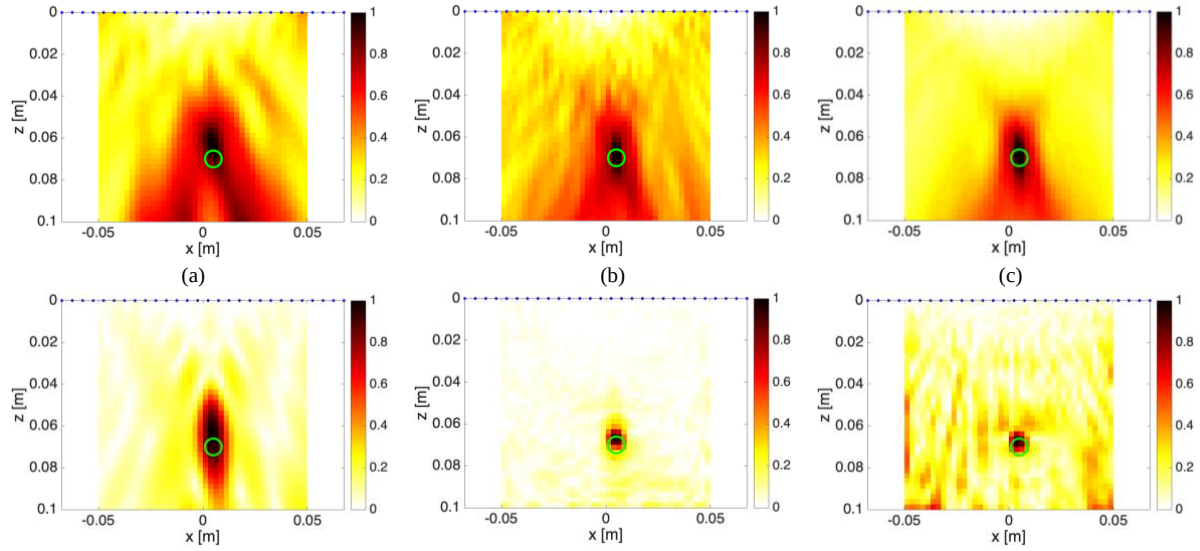

Figure 5. *Measure1*. Normalized LSM (first row) and BA (second row) indicators. (a),(d) Single-frequency processing at 18 GHz. Multi-frequency processing involving a frequency range of [18-40] GHz: (b),(e) N_F=56; (c), (f) N_F=6. The target is superimposed as a green circle, while the antenna positions are depicted as blue points.

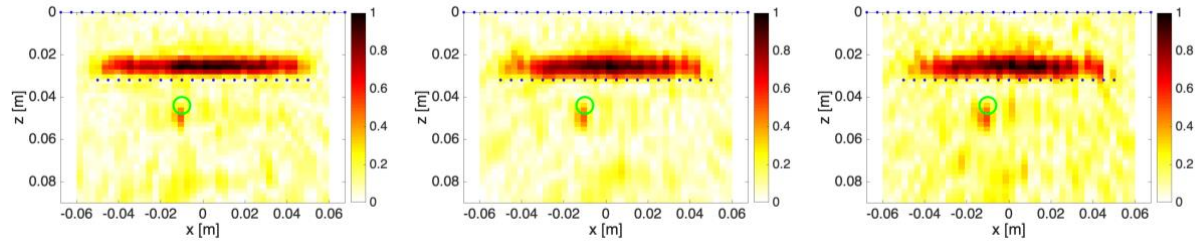

Figure 6. *Measure2*. Normalized multifrequency BA indicators. (a) f=[18-40] GHz and N_F=138, (b) f=[18-35] GHz and N_F=49, (c) f=[18-35] GHz and N_F=25. The target is superimposed as a green circle, while the antenna and air-phantom interface positions are depicted as blue points.

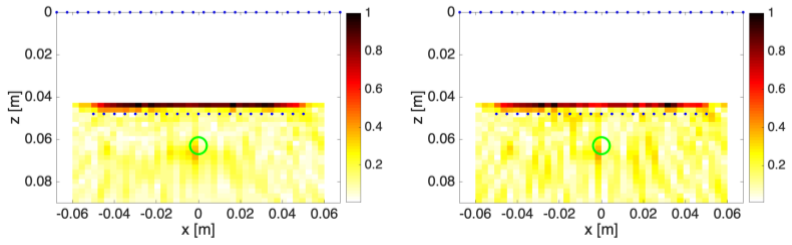

Figure 7. *Measure3*. Normalized multifrequency BA indicators. (a) [18-40] GHz and N_F=276, (b) [18-40] GHz and N_F=138. The target is superimposed as a green circle, while the antenna and air-phantom interface positions are depicted as blue points.

V. Conclusion

In this paper, inverse scattering techniques are proposed and preliminary tested against mm-wave breast cancer imaging. In particular, two of the most popular inverse scattering techniques have been adopted, that are the Linear Sampling and the Born Approximation methods.

The results have shown that both methods can allow to correctly identify the target positions up to 4 cm (from the antenna array) in the simulated scenario and 1.5 cm (from the air-phantom interface) in the experimental case. In particular, better and reliable results are obtained using the BA, especially in case of lossy and complex scenarios. With respect to radar-based techniques, so far adopted in mm-wave breast cancer imaging [20]-[24], the adopted inverse scattering techniques turn out to be more versatile and robust with respect to the reduction of the number of processed frequencies and the signal bandwidth. This represents a relevant aspect, that could imply a less complex and expensive measurement setup as well as shorter acquisition and processing time.

The interesting results presented in this paper pave the way for a better and deeper analysis of inverse scattering techniques for mm-wave imaging. Future works can be devoted at the extension of the analysis to the case of different measurement setups, for instance conformal antenna arrays. Moreover, being inverse scattering techniques able to electromagnetic characterize the target,

one could also identify its benign or malignant nature. A possible idea consists also in combining instead the advantages of both radar and inverse scattering techniques and, thus, introducing a hybrid approach.

REFERENCES

[1] Web site, accessed June 10, 2020: American Institute for Cancer Research: https://www.wcrf.org/dietandcancer/breast-cancer.

[2] S. Di Meo, *et al.*, "Correlation Between Dielectric Properties and Women Age for Breast Cancer Detection at 30 GHz", *2018 IEEE International Microwave Biomedical Conference* (*IMBioC*), Philadelphia, PA, USA, June 14-15, 2018.

[3] N. K. Nikolova, "Microwave imaging for breast cancer," *IEEE Microw. Mag.*, vol. 12, no. 7, pp. 78–94, Dec. 2011.

[4] D. O'Loughlin, *et al*, "Microwave Breast Imaging: Clinical Advances and Remaining Challenges," *IEEE Transactions on Biomedical Engineering*, Vol. 65, No. 11, pp. 2580-90, Nov. 2018.

[5] M. Lazebnik *et al.*, "A large-scale study of the ultrawideband microwave dielectric properties of normal breast tissue obtained from reduction surgeries," *Phys. Med. Biol.*, vol. 52, no. 10, pp. 2637–2656, Oct. 2007.

[6] M. Lazebnik *et al.*, "A large-scale study of the ultrawideband microwave dielectric properties of normal, benign and malignant breast tissues obtained from cancer surgeries," *Phys. Med. Biol.*, vol. 52, no. 20, pp. 6093–6115, Oct. 2007.

[7] A. Martellosio, *et al.*, "Dielectric properties characterization from 0.5 to 50 GHz of breast cancer tissues," *IEEE Trans. Microw. Theory Techn.*, Vol. 65, No. 3, pp. 998-1011, March 2017.

[8] S. Di Meo, *et al.*, "Dielectric properties of breast tissues: experimental results up to 50 GHz", *12th European Conference on Antennas and Propagation* (*EuCAP 2018*), London, UK, April 9-13, 2018.

[9] T. M. Grzegorczyk, P. M. Meaney, P. A. Kaufman, R. M. DiFlorio-Alexander, and K. D. Paulsen, "Fast 3-D tomographic microwave imaging for breast cancer detection," *IEEE Trans. Med. Imag.*, vol. 31, no. 8, pp. 1584–1592, Aug. 2012.

[10] M. J. Burfeindt, J. D. Shea, B. D. Van Veen, and S. C. Hagness, "Beamforming-enhanced inverse scattering for microwave breast imaging," *IEEE Trans. Antennas Propag.*, vol. 62, no. 10, pp. 5126–5132, Jun. 2009.

[11] H. Bahramiabarghouei, E. Porter, A. Santorelli, B. Gosselin, M. Popovic, and L. A. Rusch, "Flexible 16 antenna array for microwave breast cancer detection," *IEEE Trans. Biomed. Eng.*, vol. 62, no. 10, pp. 2516–2525, Oct. 2015.

[12] P. M. Meaney, *et al.*, "A Clinical Prototype for Active Microwave Imaging of the Breast," *IEEE Transactions on Microwave Theory and Techniques*, Vol. 48, no. 11, pp. 1841-1853, Nov. 2000.

[13] M. Klemm, I. J. Craddock, J. A. Leendertz, A. Preece, and R. Benjamin, "Radar-based breast cancer detection using a hemispherical antenna array—Experimental results," *IEEE Trans. Antennas Propag.*, vol. 57, no. 6, pp. 1692–1704, Jun. 2009.

[14] E. C. Fear, *et al.*, "Microwave breast imaging with a monostatic radar based system: A study of application to patients," *IEEE Trans. Microw. Theory Techn.*, Vol. 61, no. 5, pp. 2119–2128, May 2013.

[15] M. Klemm, I. J. Craddock, and A. W. Preece, "Contrast-enhanced breast cancer detection using dynamic microwave imaging," in Proc. IEEE Antennas Propag. Soc. Int. Symp., Chicago, IL, USA, Jul. 2012, pp. 1–2.

[16] F. Töpfer and J. Oberhammer, "Millimeter-wave tissue diagnosis: The most promising fields for medical applications," IEEE Microw. Mag., vol. 16, no. 4, pp. 97–113, May 2015.

[17] E. Porter, M. Coates, M. Popovic, "An Early Clinical Study of Time-Domain Microwave Radar for Breast Health Monitoring," *IEEE Trans. Biomed. Eng.*, Vol. 63, no. 3, pp. 530-9, Mar. 2016.

[18] K. Nemez, A. Baran, M. Asefi and J. LoVetri, "Modeling Error and Calibration Techniques for a Faceted Metallic Chamber for Magnetic Field Microwave Imaging," in *IEEE Transactions on Microwave Theory and Techniques*, vol. 65, no. 11, pp. 4347-4356, Nov. 2017.

[19] P. E. Summers, *et al.*, "Towards mm-wave spectroscopy for dielectric characterization of breast surgical margins," *ELSEVIER The Breast*, Vol. 45, pp. 64-69, June 2019.

[20] S. Di Meo, *et al.*, "On the Feasibility of Breast Cancer Imaging Systems at Millimeter-Waves Frequencies," *IEEE Transactions on Microwave Theory and Techniques* (*IEEE T-MTT*), vol. 65, no. 5, pp. 1795–1806, May 2017.

[21] S. Di Meo, *et al.*, "Tissue-mimicking materials for breast phantoms up to 50 GHz", *Phys. Med. Biol.*, Vol. 64, 055006, Feb. 2019.

[22] S. Di Meo, *et al.*, "Tissue mimicking materials for breast phantoms using waste oil hardeners," *13th European Conference on Antennas and Propagation* (*EuCAP 2019*), Krakow, Poland, March 31-April 5, 2019.

[23] S. Di Meo; G. Matrone; M. Pasian, "Experimental Validation on Tissue-Mimicking Phantoms of Millimeter-Wave Imaging for Breast Cancer Detection," *Applied Sciences*, **2021**, *11*, 432. https://doi.org/10.3390/app 11010432

[24] S. Di Meo, *et al.*, "High-Resolution mm-Wave Imaging Techniques and Systems For breast Cancer Detection", *IEEE MTT-S IMWS*, Pavia, Italy, September 20-22, 2017.

[25] D. Colton and R. Kress. Inverse Acoustic and Electromagnetic Scattering Theory, *Springer-Verlag*, Berlin, Germany, 1998.

[26] M. Bevacqua, *et al.*, "Potentialities of Inverse Scattering Techniques for Breast Cancer Imaging at Millimeter-Waves Frequencies," *14th European Conference on Antennas and Propagation* (*EuCAP 2020*), virtual conference.

[27] D. Colton, H. Haddar, and M. Piana, The linear sampling method in inverse electromagnetic scattering theory, *Inverse Problems*, 19: 105–137, 2003.

[28] A. J. Devaney, "Geophysical diffraction tomography," *IEEE Trans. Geosci. Remote Sensing*, vol. GE-22, no. 1, pp. 3–13, 1984.

[29] O. M. Bucci and Isernia T., "Electromagnetic inverse scattering: Retrievable nformation and measurement strategies", *Radio Sci*., 32: 2123–2138, 1997.

[30] M. Bertero and P. Boccacci, Introduction to Inverse Problems in Imaging, *Institute of Physics*, Bristol, UK, 1998.

[31] Catapano, L. Crocco, and T. Isernia. "On simple methods for shape reconstruction of unknown scatterers", IEEE Trans. Antennas Propag., 55:1431-1436, 2007.

[32] I. Catapano, L. Crocco, and T. Isernia, "Improved sampling methods for shape reconstruction of 3-D buried targets," IEEE Transactions on Geoscience and Remote Sensing, vol. 46, no. 10, pp. 3265-3273, 2008.

[33] M. L. Dennison and A.J. Devaney, "Inverse scattering in inhomogeneous background media: II. Multi-frequency case and SVD formulation", *Inverse Probl.*, Vol. 20, pp. 1307-1324, 2004.

[34] M. T. Bevacqua and T. Isernia, "Boundary Indicator for Aspect Limited Sensing of Hidden Dielectric Objects," in *IEEE Geoscience and Remote Sensing Letters*, vol. 15, no. 6, pp. 838-842, June 2018.